JOURNAL OF MATERIALS RESEARCH AND TECHNOLOGY 2022;16:1445–1457

Available online at www.sciencedirect.com

jmr&t Journal of Materials Research and Technology

journal homepage: www.elsevier.com/locate/jmrt

Original Article

Modelling the formation of austenite in the intercritical interval in ductile iron

Harold D. Machado [a], *Isaac Toda-Caraballo* [b], *Carlos Garcia-Mateo* [b], *Ricardo Aristizábal-Sierra* [a,*]

[a] *Gipimme; Department of Materials Engineering, Engineering Faculty, Universidad de Antioquia, Calle 67 No. 53-108, Bloque 18, Oficina 240, Medellin, 050010, Colombia*

[b] *MATERALIA Research Group, Department of Physical Metallurgy, National Center for Metallurgical Research (CENIM-CSIC), Avenida Gregorio Del Amo, 8, Madrid, 28040, Spain*

ARTICLE INFO

Article history:
Received 4 November 2021
Accepted 14 December 2021
Available online 21 December 2021

Keywords:
Intercritical austenitizing
Austenite formation
Intercritically austempered ductile iron
Austempered ductile iron

ABSTRACT

In this work, the formation of austenite in the intercritical interval under continuous heating and isothermal holding in ductile iron with various chemistries was investigated using high-resolution dilatometry and quantitative metallographic analysis. The study was conducted using fully ferritic and fully pearlitic matrices as initial microstructures. Subsequently, a mathematical model based on Avrami's equation, that describes the formation of austenite at the intercritical range, was proposed and adjusted to the experimental data. The results show that austenite formation at the intercritical range is faster and happens at lower temperatures when the initial microstructure is pearlitic. Additionally, the kinetic of austenite formation did not change by adding Cu and it is accelerated by adding Ni to the alloy. Finally, the Avrami's equation allowed to model the austenite formation under continuous heating followed by isothermal holding with a good adjustment to the experimental data, which contributes to the understanding of the kinetic of austenite formation in ductile iron at the intercritical range.

1. Introduction

Intercritically austempered ductile iron (IADI) and intercritically austenitized quenched and tempered ductile iron (IAQ&TDI) -also known as dual phase austempered ductile iron (DPADI) and dual phase ductile iron (DPDI), respectively [1–3]-, exhibit an interesting combination of mechanical properties and excellent castability and machinability, with applications for the production of powertrain and safety components [4–8].

The heat treatment to manufacture IADI and IAQ&TDI starts with an intercritical austenitization, where ferrite, austenite, and graphite coexist. Afterwards, the alloy can be austempered, to produce IADI with a microstructure consisting on graphite nodules in a matrix of proeutectoid ferrite plus ausferrite (bainitic ferrite plus high carbon austenite) [1,4–7], or quenched and tempered, to produce IAQ&TDI with a

* Corresponding author.
E-mail address: ricardo.aristizabal@udea.edu.co (R. Aristizábal-Sierra).

https://doi.org/10.1016/j.jmrt.2021.12.072

microstructure of graphite nodules in a matrix of proeutectoid ferrite plus tempered martensite [2,3,8].

The mechanical properties of IADI and IAQ&TDI depend mostly on the amount of austenite transformed after heat treatment. In general, increasing the fraction of ausferrite/tempered martensite in the matrix, increases the mechanical strength and decreases ductility [7–16]. However, controlling the amount of austenite at the intercritical range is challenging [17,18] since it depends on several factors such as chemical composition of the alloy [19], austenitization temperature [7–9], starting microstructure [20] austenitization time and heating rate [21,22]. Therefore, studying the kinetics of austenite formation during the intercritical austenitization step of the heat treatment becomes critical for the future development of this kind of ductile iron.

There are limited available studies of the kinetic of austenite formation in ductile iron at the intercritical range, however some research related to the formation of austenite during fully austenitization are available [21–23]. Abdollahi et al. [21], studied the formation of austenite in unalloyed ductile iron with a fully pearlitic starting microstructure. They evaluated the formation of austenite as a function of time at different temperatures above the upper critical austenite formation temperature using standard metallographic techniques. The austenite formation kinetics was explained by using Avrami's equation, and the corresponding kinetic parameters were fitted. Vásquez-Goméz et al. [22], studied the austenite formation kinetics in unalloyed ductile iron with a ferritic-pearlitic starting matrix using dilatometry measurements. They determined the kinetic parameters *K* and *n*, of the Avrami's equation and constructed a continuous heating transformation diagram using different heating rates for an austenitization temperature of 1000 °C. Batra et al. [23] developed a model to calculate the time required to achieve fully austenitization under para-equilibrium conditions in ductile iron austenitized at 900 °C. The model was validated by using three different ductile iron alloys with reasonable agreement.

This paper presents the study of the formation of austenite at the intercritical interval for ductile iron with various chemical compositions, and with fully ferritic and fully pearlitic starting matrices. The research was performed using high-resolution dilatometry and quantitative metallographic techniques. The experimental data was used to propose a mathematical model based on the Avrami's equation, which allows calculating the fraction of austenite formed at the intercritical range as a function of time. The kinetic parameters of Avrami's equation are then related to chemistry, intercritical austenitization temperature and starting matrix.

2. Methodology

2.1. Materials

Ductile iron and low carbon steel scrap, low-sulfur graphite and ferrosilicon were used to prepare 50 kg of each ductile iron-base alloy in an induction furnace. The copper and nickel concentration were adjusted by adding electrolytic copper and 50%Ni-ferronickel. Magnesium treatment (2 wt%) and inoculation (0.4 wt%) were performed in an open ladle using a magnesium ferrosilicon alloy (6.5 wt% Mg) and a ferrosilicon-based inoculant (2.7 Ca, 1.5 Al, 2.0 Zr y 0.01 Ce, wt%). Post-inoculation (0.1 wt%) was used before pouring the molds.

The composition of the alloys was determined by optical emission spectroscopy (OES) using a Bruker Q9 Magellan spectrometer and carbon was determined using a carbon Leco analyzer (LECO Ref. 523). The chemical composition of the alloys is listed in Table 1. Notice that the variations in elemental content are driven by the concentration of Cu and Ni, which are common alloying elements in austempered ductile iron (ADI) [24]. On the other hand, the concentration of additional alloying elements remains similar between alloys, thus, the experimental results allow understanding also, the role of Cu and Ni in the kinetic of the formation of austenite in the intercritical range.

Step blocks having 16 mm, 32 mm and 48 mm wall thicknesses were cast into green sand molds. Samples taken from the 16 mm thick section were annealed and normalized, to obtain fully ferritic and fully pearlitic matrices respectively, which permitted studying the effect of the starting matrix microstructure in the formation of the austenite. Nodularity and nodule count were determined according to the standard ASTM A247 [25]. For all the alloys, nodularity was above 90% and nodule count range between 300 and 320 nodules/mm^2. Fig. 1 shows light optical microscopy (Nikon MA100) representative micrographs of the Ni–Cu alloy were the graphite characteristics (Fig. 1(a)) and matrices (Fig. 1(b) and (c)) can be seen. The micrographs in Fig. 1 represent well the starting microstructures of the other alloys under study.

2.2. Austenite formation during continuous heating

Austenite formation during continuous heating was monitored in a Bahr 805A high-resolution dilatometer. Cylindrical samples 10 mm long and 4 mm in diameter were heated at 0.18°Cs^{-1} in a vacuum environment up to 1000 °C. The results allowed determining the critical temperatures of austenite formation and the intercritical interval as a function of composition and initial microstructure by studying the changes in the slope of the first derivative of the relative change length (RCL). Additional samples were heated at 0.18°Cs^{-1} to selected temperatures -which will be shown in the following sections-close and below, and within the intercritical range and subsequently quenched with helium at a rate of 100°Cs^{-1}. Afterwards, the samples were sectioned and polished using standard metallographic techniques with a final 1 μm diamond paste polish and etched with Nital 1%. The microstructure was analyzed by light optical microscopy (Nikon MA100) and scanning electron microscopy (SEM-Hitachi S48000 J) and the volume fraction of the

Table 1 – Chemical compositions of ductile cast iron (wt %).

Alloy	C	Si	Mn	P	S	Cr	Ni	Cu	Mg	CE[a]
Ni–Cu	3.45	2.70	0.18	0.01	0.007	0.04	0.88	0.60	0.042	4.35
Ni	3.53	2.68	0.18	0.01	0.006	0.04	0.93	0.01	0.041	4.42
Cu	3.45	2.72	0.18	0.01	0.006	0.04	0.12	0.64	0.039	4.36
Base	3.53	2.66	0.18	0.01	0.006	0.04	0.12	0.01	0.041	4.42

[a] Carbon Equivalent: CE=C+1/3Si.

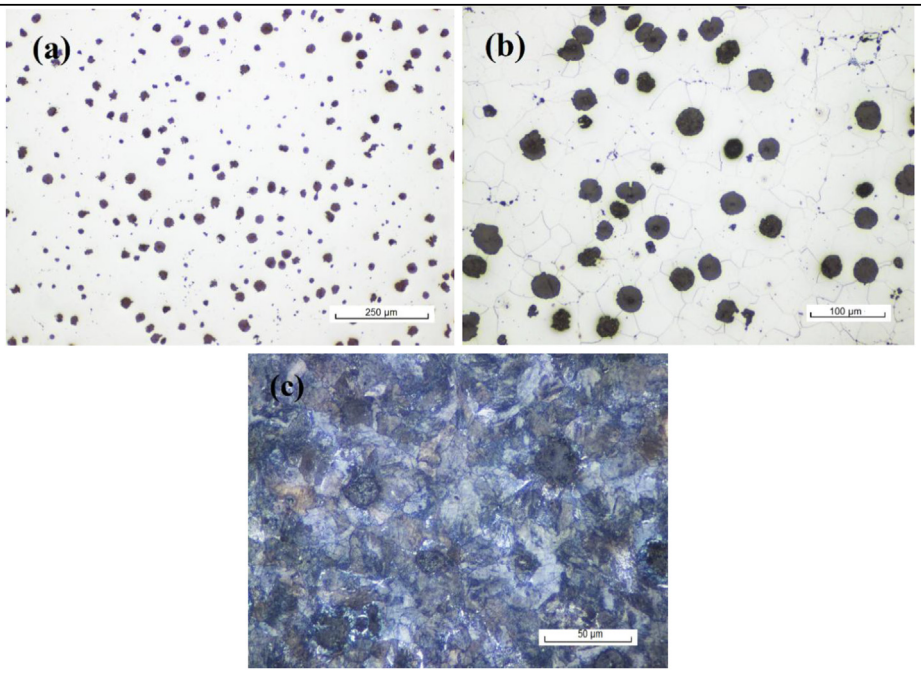

Fig. 1 – Light optical microscopy microphotos of the Ni–Cu alloy: (a) Without etching, (b) after ferritic annealing etched with Nital 1% and (c) after pearlitic annealing etched with Nital 1%.

phases was determined by systematic point counting following standard procedures [26]. SEM characterization was accomplished by using the secondary electron (SE) detector at an acceleration voltage of 7.0 kV and an average working distance of 8 mm. The volume fraction of martensite in the microstructure was taken as the volume fraction of austenite at the austenitizing temperature as it has been reported by several researchers in previous published papers [8,18,19]. Also, the volume fraction of austenite at each temperature was calculated from the dilatometric curves using the Fisher's method [27] by applying the lever rule.

2.3. *Austenite formation during isothermal holding after continuous heating*

Two temperatures in the intercritical range were selected for each alloy and each starting microstructure to evaluate the austenite formation during isothermal holding after continuous heating. The temperatures were selected, as it will be shown later, according with the results of the previous section. Samples were heated at $0.18^{\circ}Cs^{-1}$ in the dilatometer to the selected temperatures and then hold for 0, 2, 5, 15 and 30 min. After the dilatometric analysis, microstructural characterization was carried out using light optical microscopy (Nikon MA100) and SEM (SEM-Hitachi S48000 J) in samples prepared by standard metallographic techniques. Finally, the volumetric fractions of phases were determined by systematic point counting following standard procedures [26].

2.4. *Modelling the austenite formation in the intercritical range*

The volume fraction of austenite, $f(\gamma)$, obtained after isothermal holding were used to calculate the parameters K (reaction rate) and n (reaction order) in the Avrami's equation (Eq. (1)) [28,29]. The parameters K and n were fitted for the alloys and the starting microstructures under evaluation. Using the dilatometric data from the continuous heating experiments, the variation of the parameter K at each temperature ($K(T)$) in the system was calculated, where the value of n is considered constant for each alloy-initial microstructure system. After that, a numerical optimization was performed using the Nelder-Mead-Minimum method [30] to model the austenite transformation curve under continuous heating conditions using Eq. (2) and subsequently, the total fraction of austenite after continuous heating and isothermal holding was calculated by combining Eq. (1) and Eq. (2) as shown in Eq. (3).

$$f(\gamma) = 1 - e^{-Kt^n} \quad \text{Isothermal holding} \tag{1}$$

$$f(\gamma) = \left(1 - e^{-K(T)t^n}\right) \quad \text{Continuous heating} \tag{2}$$

$$f(\gamma) = \left(1 - e^{-Kt^n}\right) + \left(1 - e^{-K(T)t^n}\right) \quad \text{Isothermal holding after continuous heating} \tag{3}$$

Table 2 – Critical austenite transformation temperatures.

Initial microstrucutre	Alloy	T_S (°C)	T_F (°C)	Intercritical Interval under continuous heating, (T_F-T_S), (°C)
Ferritic	Ni–Cu	797	927	130
	Ni	793	878	85
	Cu	796	896	100
	Base	792	883	91
Pearlitic	Ni–Cu	780	845	65
	Ni	784	853	69
	Cu	787	851	64
	Base	784	845	61

3. Results and discussion

3.1. *Austenite formation in continuous heating*

Table 2 lists the results of the determination of the austenite formation temperatures for the alloys under study. Fig. 2 shows the results of the dilatometric essays for the pearlitic and ferritic initial microstructures for the Base alloy. In Fig. 2, it can be seen the regions where the transformations from ferrite to austenite (Fig. 2(a)) and from pearlite to austenite (Fig. 2(b)) are taking place. The vertical dashed lines in Fig. 2 indicate the austenite formation start temperature (T_S) and the austenite formation finish temperature in continuous heating (T_F) [31,32], which were determined by examining the changes in the slope of the first derivative of the relative change in length (d (RCL)/dL). The determination of T_S and T_F were corroborated by examining the microstructure of samples austenitized at different temperatures, as it will be shown later in Figs. 3 and 4.

Results in Fig. 2(a) show that when the initial microstructure is ferritic, the formation of the austenite leads to the continuous increase in the RCL, which is related to the increase in the atomic volume as the matrix goes from ferrite to austenite. Also, it can be seen in Fig. 2(b) that when the transformation goes from pearlite to austenite, the change in the RCL is stronger, which is linked to the dissolution of iron carbides in the cementite, which have a larger atomic volume than austenite [33], and the formation of ferrite halos around the graphite nodules.

T_S and T_F in ferritic initial microstructures occur at higher temperatures than in pearlitic initial microstructures. The

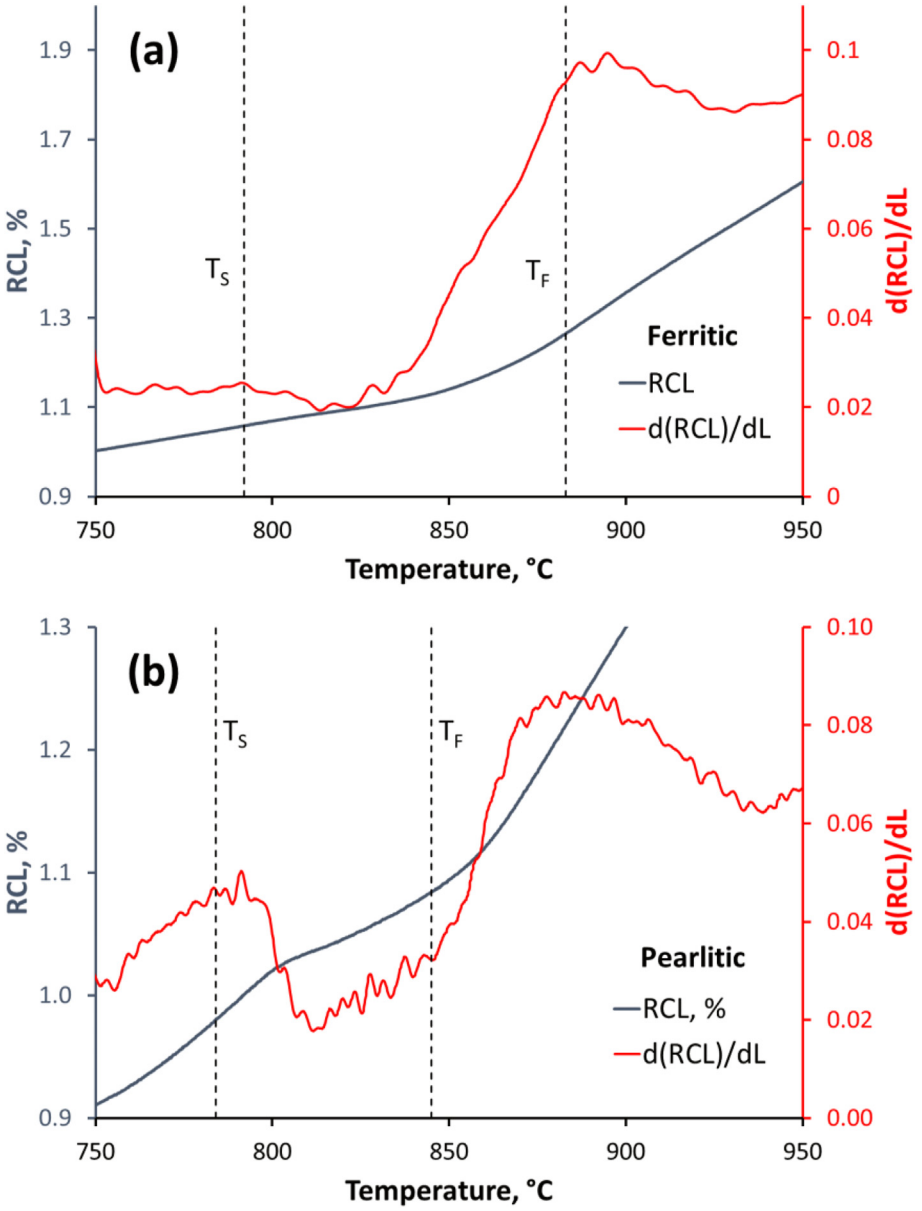

Fig. 2 – Dilatometric curves and first derivatives for the Base alloy with (a) ferritic and (b) pearlitic initial microstructures. T_S and T_F are indicated by vertical dashed lines according to the changes in the slope of the first derivative of the RCL.

differences in T_S are attributed to the fact that austenite nucleation occurs much faster in the pearlitic colonies, where there are more nucleation sites, and the available carbon is greater than in ferritic matrices [34]. As for T_F, the differences between the ferritic and pearlitic microstructures are mainly due to carbon diffusion, in ferritic microstructures carbon is only available in the graphite nodules, while in pearlitic microstructures carbon is available also in the carbides of the pearlite, in addition to the graphite nodules. Also, the diffusion distance of the carbon during the decomposition of the pearlite is smaller than the diffusion distance of carbon from the graphite nodules, so its diffusion will take less time in the pearlitic microstructures.

It has to be recalled that the energy required to start the transformation depends mainly on the heating rate, the starting microstructure, and the alloying elements that can delay the austenitic transformation (in this case Si and Cu) [35–37]. When there is pearlite in the ductile iron microstructure, T_S is closer to the metastable eutectoid temperature, indicating that the kinetics of austenite formation is mainly related to the boundaries of the pearlite colonies and the pearlite interlaminar spacing [38,39]. This phenomenon does not occur with the formation of austenite from a ferritic initial microstructure, which is controlled by the diffusion of C under paraequilibrium conditions [38,39]. Although austenite growth is known to be much faster into the ferritic grains, the rate of austenite formation in cast irons could be lower due to the high concentration of Si, which decreases the mobility of C atoms at temperatures close to the eutectoid temperature, increasing T_S, which become closer to the stable equilibrium eutectoid temperature, and increasing the intercritical interval under continuous heating conditions [40].

Figs. 3 and 4 show representative optical micrographs of the Ni–Cu alloy with pearlitic and ferritic initial microstructures respectively. The samples were continuously heated in the dilatometer at $0.18°Cs^{-1}$ to selected temperatures and then quenched. These sequences of micrographs represent qualitatively well, the series of events observed in the other alloys under study. Regarding the samples with initial pearlitic microstructures in Fig. 3, at 750 °C the microstructure was mostly pearlitic with the formation of ferrite halos around the graphite nodules. Notice that the ferrite halos are the product

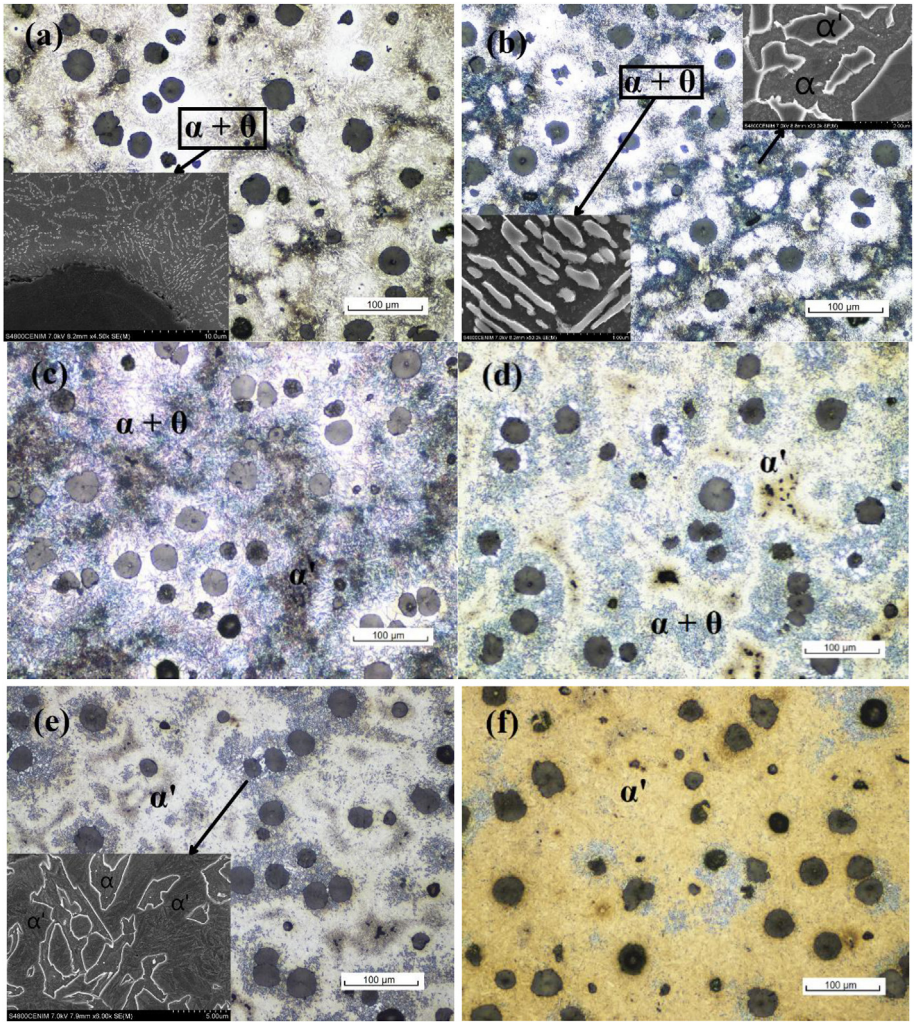

Fig. 3 – For the Ni–Cu alloy with initial pearlitic microstructure, evolution of the quenched microstructure after continuous heating at a) 750 °C, b) 780 °C, c) 790 °C, d) 800 °C, e) 820 °C, f) 840 °C. Where α: ferrite, α+θ: pearlite and α': martensite. Etched with Nital 1%.

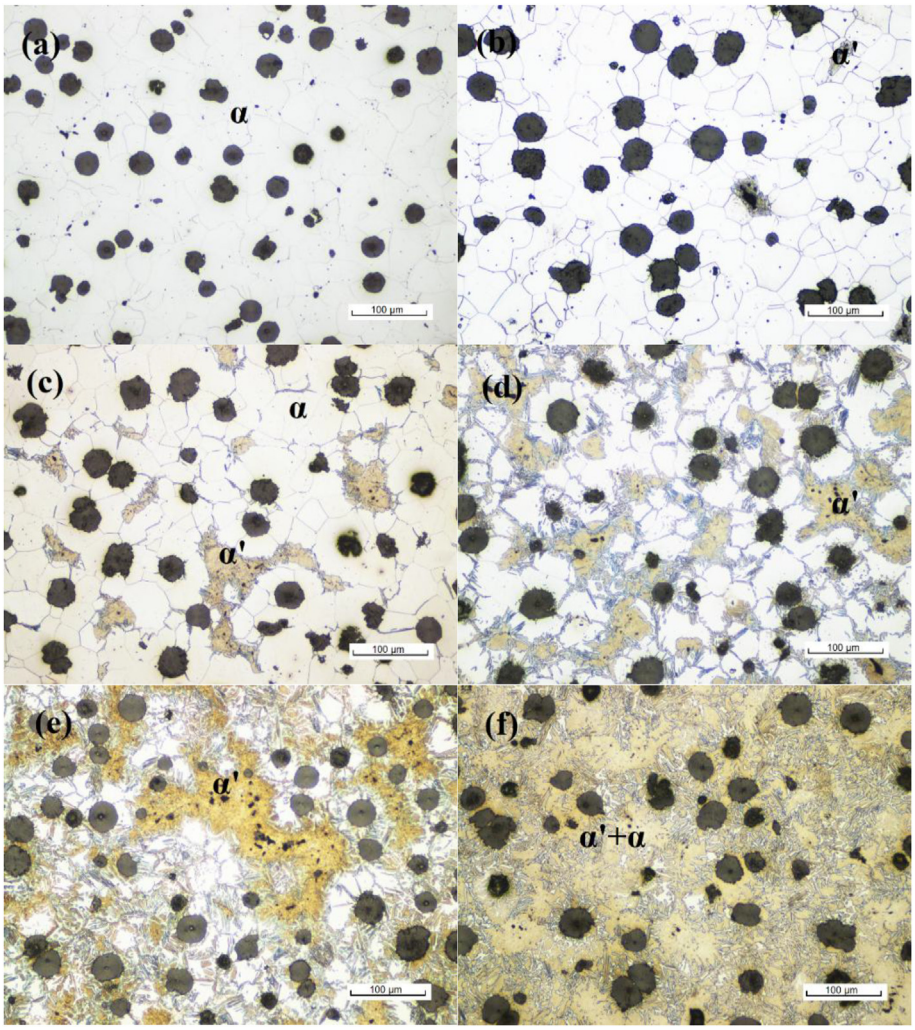

Fig. 4 – For the Ni–Cu alloy with initial ferritic microstructure, evolution of the quenched microstructure after continuous heating at a) 780 °C, b) 800 °C, c) 820 °C, d) 840 °C, e) 860 °C, f) 880 °C. Where α: ferrite (white phase) and α': martensite (brown phase). Etched with Nital 1%.

of the diffusion of carbon from the decomposition of cementite, towards the graphite nodules, supported by the effect of silicon microsegregation in the nodule contour

Table 3 – Volume percent of austenite as a function of temperature under continuous heating obtained by systematic point counting.

Pearlitic initial microstructure				
Temperature, °C	790	800	820	840
Ni–Cu, vol%	15.5 ± 2.5	66.9 ± 1.1	80.0 ± 2.1	90.2 ± 2.0
Ni, vol%	–	32.6 ± 1.2	41.6 ± 1.2	89.5 ± 3.0
Cu, vol%	–	5.6 ± 1.2	66.6 ± 1.4	84.4 ± 3.5
Base, vol%	–	4.7 ± 0.8	56.0 ± 1.8	84.2 ± 2.4

Ferritic initial microstructure					
Temperature, °C	800	820	840	860	880
Ni–Cu, vol%	3.3 ± 0.8	12.8 ± 2.7	28.7 ± 2.4	65.8 ± 2.8	87.3 ± 3.1
Ni, vol%	8.5 ± 1.5	14.5 ± 1.2	35.7 ± 1.6	61.1 ± 3.1	84.9 ± 3.1
Cu, vol%	3.6 ± 0.5	15.4 ± 1.4	25.0 ± 2.9	56.2 ± 1.7	75.9 ± 1.8
Base, vol%	3.5 ± 0.9	5.5 ± 1.7	25.5 ± 2.4	61.2 ± 3.2	75.4 ± 2.1

[41,42], since at 750 °C the austenite formation has not started yet (see Table 2). At 780 °C and 790 °C the microstructure contains ferrite, pearlite and small islands of martensite, which form in the intermediate areas between the primary graphite nodules. The total dissolution of the pearlite is only reached between 800 °C and 820 °C, the micrographs in Fig. 3(d) and (e) show lesser iron carbides from the pearlite and an increase in the ferrite and martensite volume fractions as the temperature increases. The highest formation of austenite occurs between 820 °C and 840 °C, at this latter temperature the microstructure is almost completely martensitic and only small ferrite islands remain around the graphite nodules.

Concerning the samples with initial ferritic microstructures in Fig. 4, at 780 °C the microstructure consists of graphite nodules in a ferritic matrix and there is no presence of martensite, indicating that the formation of the austenite has not yet started, as expected from the data in Table 2. At 800 °C, there are small islands of martensite (the light brown phase in Fig. 4(b)–(f)) at the intermediate zones between the primary graphite nodules. Based on the transformation start temperatures for ferritic matrices previously discussed (Table 2), the

intercritical interval starts between 790 °C and 800 °C. The austenite begins to grow from the grain boundaries towards the interior of the ferrite grains, the amount of austenite formed will depend mainly on the diffusion of carbon and the microsegregations in the matrix, as seen in the micrograph of the sample quenched from 840 °C in Fig. 4(d). At 860 °C there is still ~30% volume of ferrite and finally only until the alloy reaches 880 °C the matrix become almost completely martensitic with small grains of ferrite at the contours of the graphite nodules, which indicates that around this temperature the intercritical interval is ending in continuous heating when the austenitization starts from a ferritic matrix.

As mentioned before, the previous description of the microstructural evolution for the Ni–Cu alloy also applies to the other alloys under study. However, as shown in Table 2, the critical temperatures vary slightly according to the alloy, as it does the volumetric fractions of formed austenite. Table 3 shows the results of the quantification by systematic point counting of the austenite volume fraction in continuous heating in the intercritical range for all the alloys. Fig. 5 shows with solid lines the volumetric fraction of austenite formed for ferritic and pearlitic initial microstructures of the alloys under study calculated using the Fisher's method and the data from the dilatometric tests. The results are compared with the volumetric fractions in Table 3, which are presented in Fig. 5 using dots with their respective standard deviation. As it can be seen, the calculated austenite volumetric fraction using the dilatometric results adjusts well with the data in Table 3. The observed deviations can be associated with microstructural effects that affect the RCL and that are not considered by Fisher's method such as: the C enrichment of austenite, the increase in the volumetric fraction of graphite due to the migration of C to the nodules, the formation of temper graphite in the pearlitic samples and, the formation of ferrite halos around the graphite nodules in the pearlitic samples. For all the alloys, it is observed that austenite formation occurs faster and at lower temperatures when the starting matrix is pearlitic. The results show from the dilatometric data that the fractions of austenite formed under continuous heating can be estimated with good accuracy.

3.2. *Austenite formation in the intercritical range during isothermal holding after continuous heating*

Fig. 6 shows representative micrographs of the Ni–Cu alloy isothermally hold at the intercritical range during 0, 2, 5, 15 and 30 min, for the pearlitic and ferritic initial microstructures. The sequences of transformation events are similar for the other alloys and temperatures under study. When the initial microstructure is ferritic, austenite formation starts in the grain boundaries at the last freezing zones between the primary graphite nodules, which agrees with the reports of other researchers [17,18]. After that, austenite formation continues through the grain boundaries and some austenite branches start to connect with the graphite nodules. These austenite branches widen as the isothermal holding time reaches 15 and 30 min. As for the samples with initial pearlitic microstructures, the results show that austenite formation starts at the last freezing zones as well, but some austenite is also observed close to the graphite nodules showing a more even distribution of the austenitic phase in the matrix. After 5 min of isothermal holding, ferritic halos around the graphite nodules are well defined and some austenite has been formed at the ferritic grain boundaries close to the graphite nodules. Finally, after 15 min and up to 30 min the ferrite halos disappear and only some small ferritic islands close to the graphite nodules remain.

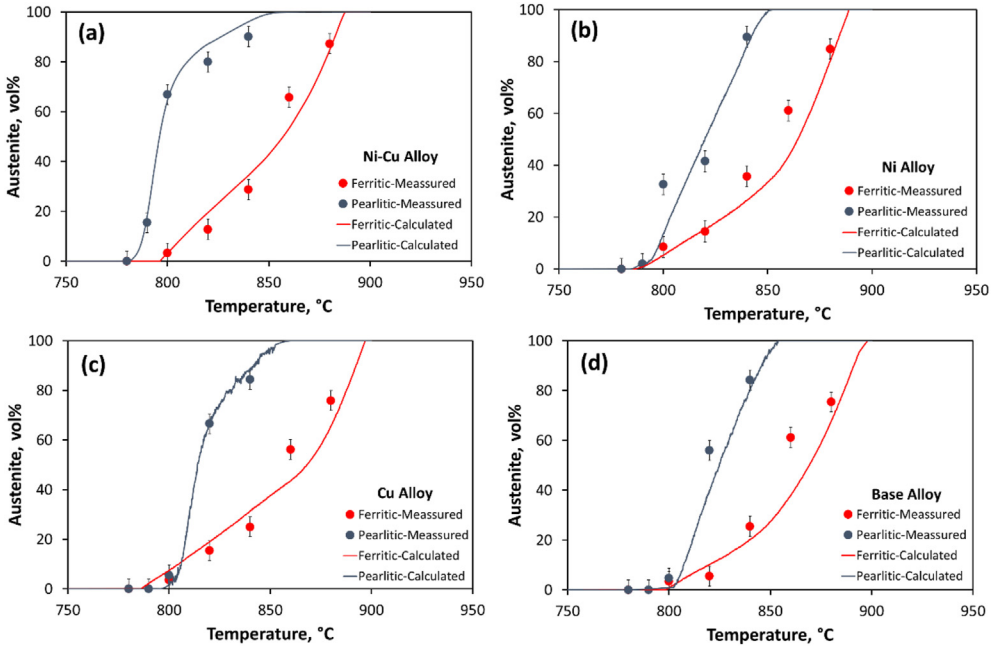

Fig. 5 – Volume percent of austenite as a function of temperature in continuous heating calculated from the dilatometric essays using the Fisher's method and experimentally determined by metallographic point counting: a) Ni–Cu alloy, b) Ni alloy, C) Cu alloy and D) Base alloy.

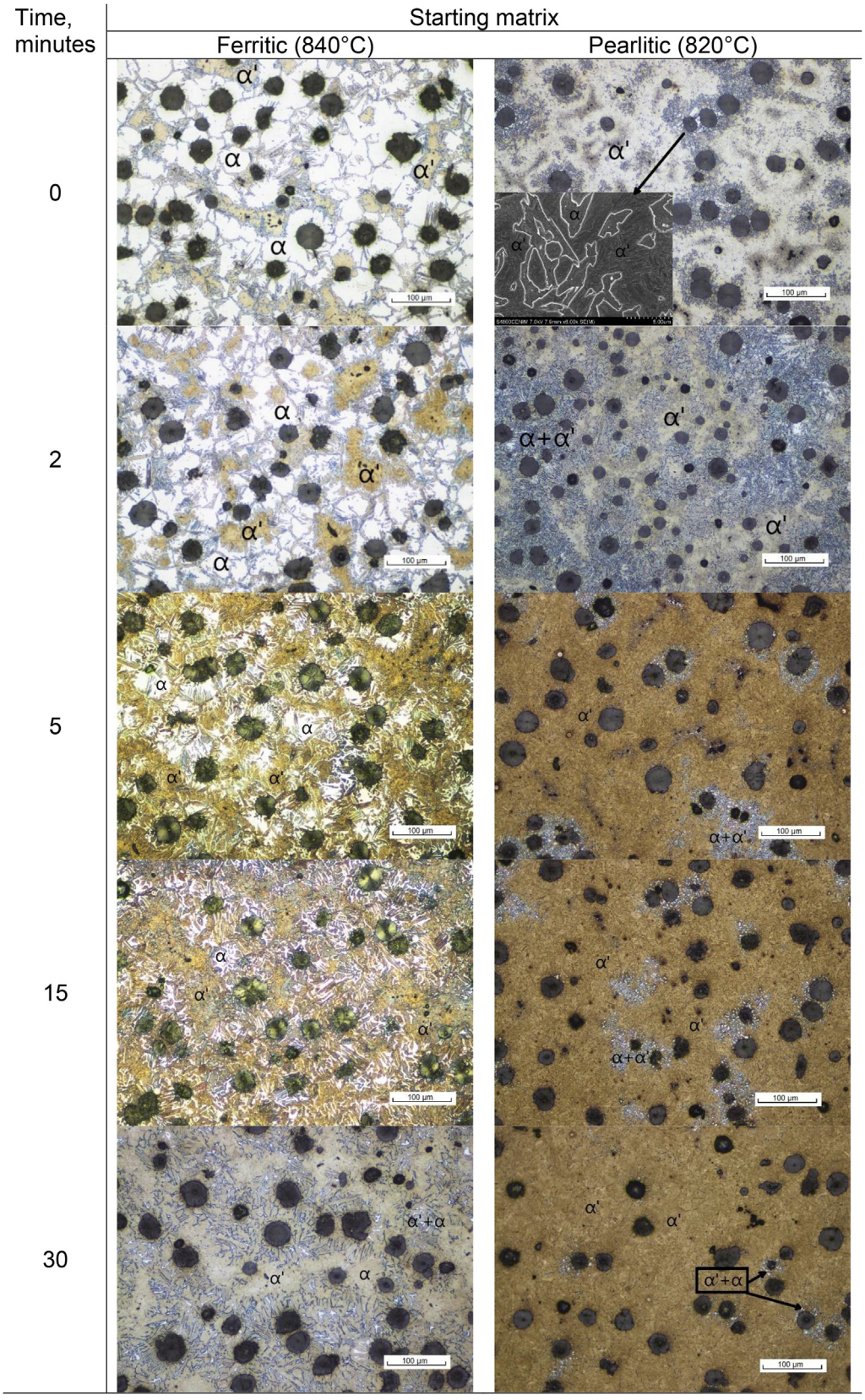

Fig. 6 – Representative micrographs of the evolution of the microstructure as function of the holding time for the Ni–Cu alloy intercritically austenitized and with fully ferritic and fully pearlitic starting matrices. Where α: ferrite (white phase), α': martensite (brown phase). The blue areas in the micrographs are a fine mixture of α+α'. Etched with Nital 1%.

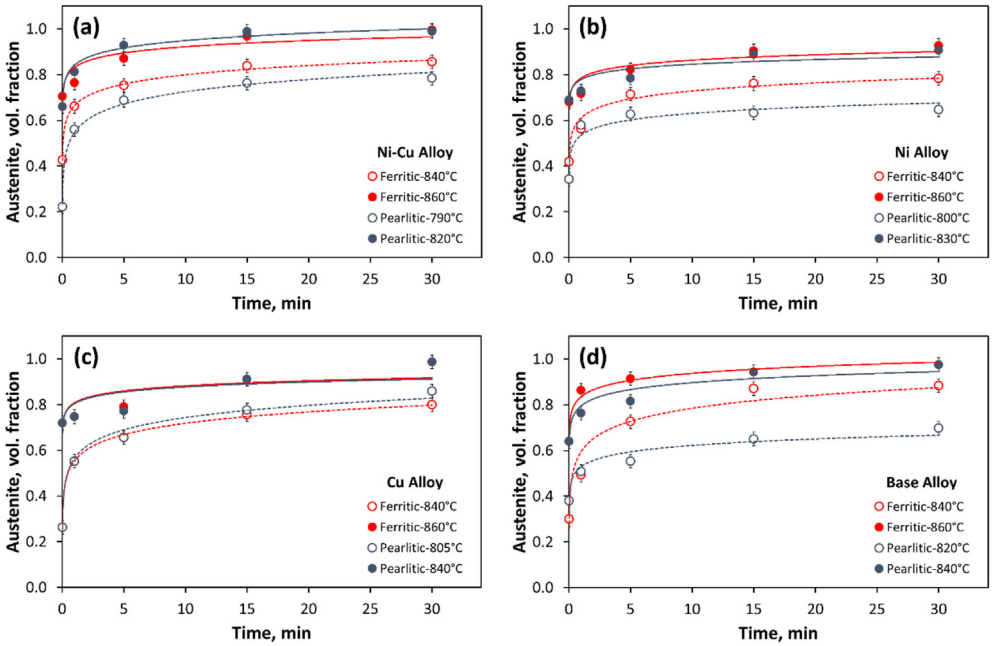

Fig. 7 – Austenite volume fraction for isothermal holding after continuous heating. (a) Ni–Cu alloy, (b) Ni alloy, (c) Cu alloy and (d) Base alloy.

The results show that austenite formation is fast at the beginning of the isothermal holding and slows down after 15 min for both initial microstructures, ferritic and pearlitic. The differences between the ferritic and the pearlitic initial microstructures samples arrive from the need of initially dissolving the cementite in the pearlite, which in turn causes the growth of the ferritic phase. When the cementite dissolves completely, only ferrite and austenite will be present in the matrix. The process of dissolving the cementite is intimately related with the austenitizing temperature and takes more time when the temperature is close to T_S. For example, Lopes [17], and Guesser et al. [18] have reported that even after 12 h of isothermal holding at 790 °C some spheroidized carbides remain in the microstructure of ductile iron. On the other hand, when the initial microstructure is ferritic, the transformation will go directly from ferrite to austenite, therefore, by increasing the temperature or the holding time, the diffusion of carbon in the matrix will increase [25], which will imply a growth of the austenitic phase and a decrease in the volume fraction of ferrite.

Fig. 7 shows the evolution of the fraction of austenite as a function of isothermal holding time for the alloys, holding temperatures and initial microstructures under study. Notice that the holding temperatures were selected within the intercritical range according to the results of the previous section. For all the cases, the amount of austenite increased rapidly during the first 5 min of isothermal holding. After that, the amount of austenite increased more slowly and in almost all the cases under evaluation reached a stable value after 15 min of intercritical austenitization. As expected, austenite formation was faster, and the volume fraction of austenite was higher as the intercritical austenitization temperature increased. In Fig. 7, it is worth noting that the Cu alloy and the base alloy were evaluated at 840 °C with the two initial microstructures. The results showed that austenite growth was faster and the final fraction of austenite (after 30 min of isothermal holding) was higher when the initial microstructure was pearlitic. The same trend can be observed for the other alloys under evaluation, for example the Ni–Cu alloy with an initial pearlitic microstructure gives a higher volumetric fraction of austenite at 820 °C than the same alloy with a ferritic initial microstructure intercritically austenitized at 840 °C. Similarly, the Ni alloy with a pearlitic initial microstructure reaches a higher volumetric fraction of austenite at 830 °C than the same alloy with a ferritic initial microstructure intercritically austentized at 840 °C. These results, as explained before, are related with: (1) the availability of nucleation sites, that are higher when the initial microstructure is pearlitic, which in turn accelerates austenite formation [38] and (2) the intercritical range for austenite formation which happens at lower temperatures when the initial microstructure is pearlitic [39], thus at the same intercritical austenitizing temperature the pearlitic initial microstructure will give a higher fraction of austenite.

3.3. *Modeling of the austenite formation in the intercritical interval*

The volumetric fractions of austenite obtained from the microstructural characterization of the isothermal holding experiments were used to calculate the slope of $ln(t)$ *vs* $ln(ln(1/(1-f(\gamma))))$ which gives the reaction order, n, of the Avrami's equation as shown in Eq. (1). To this end, $t = 0$ was taken as the time when the system reached Ts. The time since the beginning of the austenite formation to the zero-isothermal holding time was calculated as $(T_{iso} - Ts)/0.18$, where T_{iso} is the isothermal holding temperature and 0.18 comes from the heating rate. The results are presented in Table 4, where T_L

Table 4 – Values of the reaction order, *n*, of the Avrami's equation at the intercritical interval obtained from the isothermal holding experiments at T_L and T_H.

Initial Microstructure	Alloy			
	Ni–Cu	Ni	Cu	Base
Pearlite (T_L)	2.9	3.2	3.0	3.0
Pearlite (T_H)	3.2	3.0	3.2	3.2
Ferrite (T_L)	3.1	3.1	3.1	3.1
Ferrite (T_H)	3.2	3.1	3.2	3.2

and T_H are the lowest and the highest T_{iso} of each alloy respectively, as shown in Fig. 7. The fitted value of *n* ranges between 2.9 and 3.2, in addition, no important variation of the reaction order was observed as a function of chemical composition (which has small variations on Cu and Ni) or initial microstructure, and the variations can be attributed to the intrinsic measurement errors. Notice that the *n* values obtained are lower as compared with the results reported by other authors for fully austenitization [21,22]. For example, Abdollahi et al. [21] reports for unalloyed ductile iron with a pearlitic initial microstructure, *n* values between 4.7 and 4.9 and Vasquez-Gómez et al. [22] report *n* values close to 4 for unalloyed ferritic-pearlitic ductile iron. The reaction order is closely related with the nucleation and growth rate, usually the reaction order for austenite formation is assumed as 4, which indicates that both, nucleation and growth rate, do not change in time and that the nucleation process is not exhausted [38]. In the present case during the first stages of intercritical austenitization, nucleation and growth processes are limited to the last freezing zones, and growth goes preferentially trough the grain boundaries -as shown in the previous sections-, which may explain the lower values of *n* obtained for intercritical austenitization of ductile iron.

Modeling the heating curve in the intercritical interval requires also knowing the value of the reaction rate constant, *K*. While *n* is temperature-independent, *K* varies with temperature [22]. Thus, to model the complete system during continuous and isothermal heating, two sections were used: the first section of continuous heating has a temperature-dependent constant *K(T)* (see Eq. (2)), while the second section of isothermal holding has a *K* that was assumed constant, considering that the temperature is the same throughout the

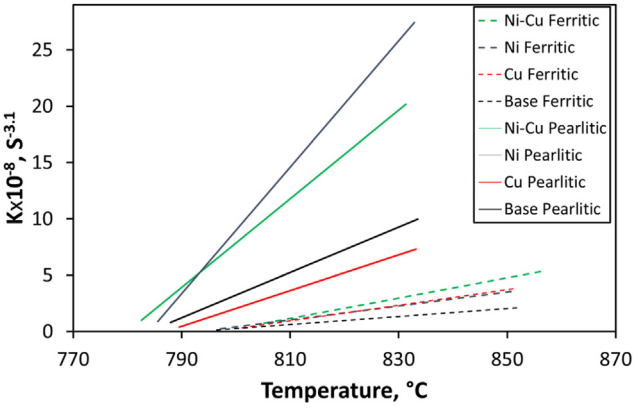

Fig. 8 – Variation of *K* as a function of temperature (*K(T)*).

treatment (see Eq. (1)). As mentioned above in the methodology, the austenite fraction formed during the entire cycle of continuous heating followed by isothermal holding was calculated according to Eq. (3). Additionally, the maximum fraction of austenite formed at the intercritical austenitization temperature was set as $(T_{iso} - T_S)/(T_F - T_S)$.

To solve the model, the average values of *n* for each alloy-initial microstructure in Table 4 were taken. It must be recalled that, as it was mentioned early *n* is temperature-independent. Notice that the *n* average for all the cases is 3.1, which emphasize that for intercritical austenitization of ductile iron, the reaction order seems not to be dependent on the initial matrix (ferrite or pearlite) and it does not change by the small additions of Cu and Ni. Additionally, to solve the model the results of the determination of the volume fraction of austenite at the intercritical range in continuous heating and the results from the isothermal experiments, were used to calculate the variation of *K* as a function of temperature and to optimize Eq. (3) using the Nelder-Mead-Minimum method [30]. The method looks for an approximate local optimal solution to a problem with N variables when the function to be optimized varies smoothly, testing all possible values for the solution of the equation.

Fig. 8 shows the variation of *K* as a function of temperature and Table 5 lists the equations that describe the variation of *K* with temperature within the intercritical range obtained after solving the model. Notice that *K* values are higher for samples with a pearlitic initial microstructure, in good agreement with the experimental results that show that austenite formation is faster for the pearlitic samples. Fig. 8 also indicates that *K* increases with temperature, which is explained because austenite formation is a diffusion driven reaction [38], thus the reaction rate is higher as the temperature raises.

Fig. 9 shows the fitting of the solution of the model with a deviation lower than 10% with respect to the austenite volumetric fraction experimental data, which are represented in the graphs as circular dots. Notice that the experimental data in Fig. 9 includes continuous heating and isothermal holding results. The time when the system goes from continuous heating to isothermal holding is indicated in the graphs by vertical lines. The results show a good fitting of the curves, which indicates that the behavior of the austenite formation in the intercritical interval can be model properly with the proposed methods and equations.

Fig. 10 compares results from simulating the intercritical austenitization at the same temperature for the alloys under

Table 5 – Equations to calculate *K* (in $s^{-3.1}$) as a function of temperature (*K(T)*).

Alloy	Starting matrix	
	Pearlitic	Ferritic
Ni–Cu	3.934×10^{-9} (T+273) - 4.142×10^{-6}	9.015×10^{-10} (T+273) - 9.646×10^{-7}
Ni	5.609×10^{-9} (T+273) - 5.929×10^{-6}	6.175×10^{-10} (T+273) - 6.583×10^{-7}
Cu	1.581×10^{-9} (T+273) - 1.675×10^{-6}	6.875×10^{-10} (T+273) - 7.349×10^{-7}
Base	2.014×10^{-9} (T+273) - 2.128×10^{-6}	3.495×10^{-10} (T+273) - 3.722×10^{-7}

evaluation. Notice that comparing the results with the Base alloy gives an indication of the effect of the alloying elements or they combination. Fig. 10(a) shows the results of simulating austenite formation at 840 °C for a ferritic initial microstructure. It can be seen that a small addition of Cu does not alter the kinetic of austenite formation even tough Cu is an austenite stabilizer. On the other hand, a small addition of Ni accelerates the kinetic of austenite formation, which may be related to the fact that Ni is a strong austenite stabilizer. Finally, the combination of Ni and Cu seems to accelerate even further the formation of austenite at the intercritical interval, which may be linked to the fact that both, Cu and Ni, are austenite stabilizers. Fig. 10(b) shows the results of simulating austenite formation at 820 °C for a pearlitic initial microstructure. Again, a small addition of Cu does not have an effect on the kinetic of austenite formation, Ni accelerates the reaction and the combination of Ni and Cu accelerates even more austenite formation.

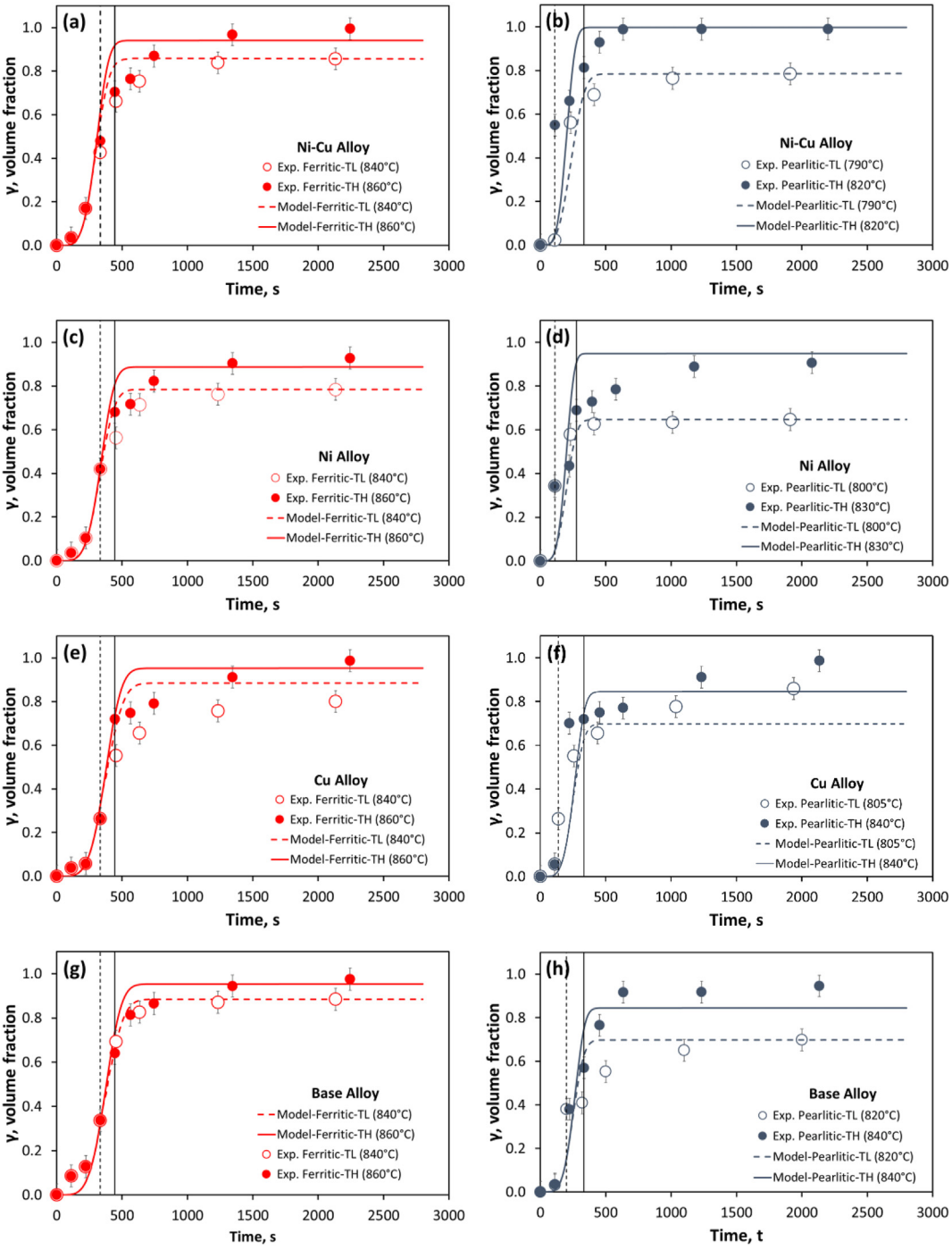

Fig. 9 – Model adjustment to the continuous heating plus isothermal holding experimental data using the Nelder-Mead-Minimum method, the vertical lines indicate the start of isothermal holding. (a) Ni–Cu-Ferritic, (b) Ni–Cu-Pearlitic, (c) Ni-Ferritic, (d) Ni-Pearlitic, (e) Cu-Ferritic, (f) Cu-Pearlitic, (g) Base-Ferritic and (f) Base-Pearlitic.

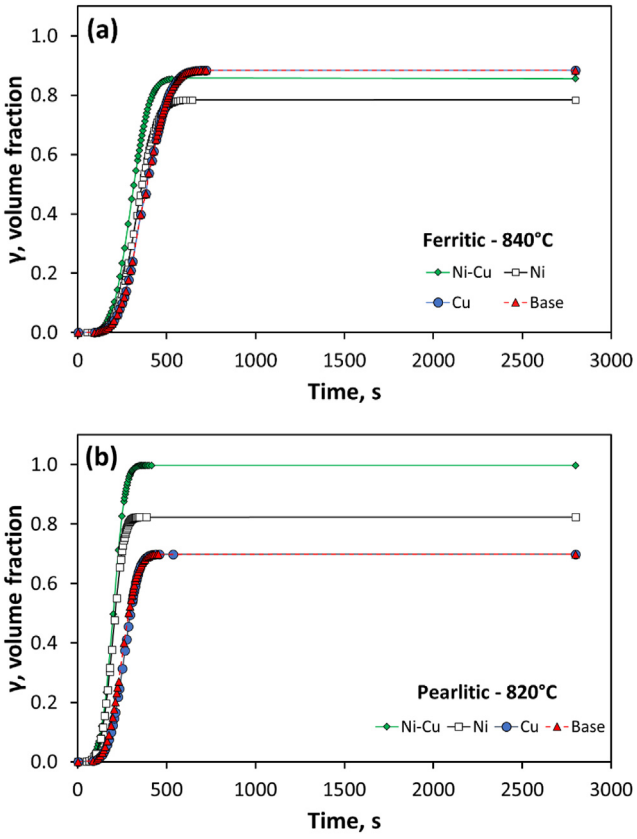

Fig. 10 – Simulation of the volume fraction of austenite as a function of time: (a) ferritic initial microstructure intercritically austenitized at 840 °C and (b) pearlitic initial microstructure intercritically austenitized at 820 °C.

4. Conclusions

Intercritically austenitization of ductile iron was studied under continuous heating and isothermal holding using four alloys with small variations in the concentration of Ni and Cu and using fully ferritic and fully pearlitic initial microstructures. The results showed that dilatometric tests and the Fisher's method can be used to estimate the volume fraction of austenite formed as a function of temperature in continuous heating with good accuracy. The experimental information was used to successfully adjust a model based on the Avrami's equation, which gives an average reaction order of 3.1 regardless of the initial matrix and chemical composition of the alloy. The calculations revealed that austenite formation is faster and happens at lower temperatures when the starting matrix is pearlitic. Also, a small addition of Cu (~0.6wt%) does not alter the kinetic of austenite formation, the addition of Ni (~0.9wt%) accelerates the reaction and the addition of both, Ni and Cu accelerates austenite formation further.

Declaration of Competing Interest

The authors declare that they have no known competing financial interests or personal relationships that could have appeared to influence the work reported in this paper.

Acknowledgments

The authors want to acknowledge COLCIENCIAS (Call 727), CODI (PRG 2017–16229) and CENIM (National Center for Metallurgical Research-Madrid-Spain).

REFERENCES

[1] Basso AD, Martínez RA, Sikora JA. Influence of austenitizing and austempering temperatures on microstructure and properties of dual phase ADI. Mater Sci Technol 2007;23(11):1321–6.
[2] Rashidi AM, Moshrefi-Torbati M. Effect of tempering conditions on the mechanical properties of ductile cast iron with dual matrix structure (DMS). Mater Lett 2000;45(3):203–7.
[3] Kocatepe K, Cerah M, Erdogan M. Effect of martensite volume fraction and its morphology on the tensile properties of ferritic ductile iron with dual matrix structures. J Mater Process Technol 2006;178(1–3):44–51.
[4] Druschitz AP, Aristizabal R, Druschitz E, Hubbard CR, Watkins TR, Walker L, et al. In situ studies of intercritically austempered ductile iron using neutron diffraction. Metall Mater Trans A 2011;43(5):1468–76.
[5] Aristizábal R, Foley RD, Andrews JB. Intercritical heat treatments in ductile iron and steel. Thesis. 2012.
[6] Druschitz A, Aristizabal R, Druschitz E, Hubbard C, Watkins T. Neutron diffraction studies of intercritically austempered ductile irons. SAE International Journal of Materials and Manufacturing 2011;4(1):111–8.
[7] Aristizabal RE, Druschitz AP, Druschitz E, Bragg R, Hubbard CR, Watkins TR, et al. "Intercritically austempered ductile iron" AFS transactions 2011, vol. 119. Schuamburg, IL: American Foundry Society; 2011. p. 407–12.
[8] Aristizabal R, Foley R, Druschitz AP. Intercritically austenitized quenched and tempered ductile iron. Int. J. Met. 2012;6(4):7–14.
[9] Hoang LV, Hong HN, Anh TH, Anh TV, Nguyen DT, Tan SJ. Influence of heat treatment processing three phase region on the microstructure and hardness ADI alloys. *J. Mech. Eng.* Res. Dev 2021;44(7):289–96.
[10] Basso A, Caldera M, Chapetti M, Sikora J. Mechanical characterization of dual phase Austempered ductile iron. ISIJ Int 2010;50(2):302–6.
[11] Cerah M, Kocatepe K, Erdogan M. Influence of martensite volume fraction and tempering time on tensile properties of partially austenitized in the ($\alpha + \gamma$) temperature range and quenched + tempered ferritic ductile iron. J Mater Sci 2005;40(13):3453–9.
[12] Aristizabal R, Hayrynen K, Foley R, Griffin J, Monroe C. Austemperability of intercritically austempered ductile iron (IADI). Int. J. Met. 2014;6(4):279–86.
[13] Panneerselvam S, Putatunda SK, Gundlach R, Boileau J. Influence of intercritical austempering on the microstructure and mechanical properties of austempered ductile cast iron (ADI). Mater Sci Eng, A 2017;694:72–80.
[14] Uyar A, Sahin O, Nalcaci B, Kilici V. Effect of austempering times on the microstructures and mechanical properties of dual-matrix structure austempered ductile iron (DMS-ADI). Int J Metalcast 2021:1–12.
[15] Chen JK, Chen BT, Tsai JS. Microstructural evolutions and properties of partially austenitizing and austempered ductile irons. Steel Res Int 2016;87(2):191–8.
[16] Ghoroghi M, Nasser V. Effect of austempering parameters on microstructure and mechanical properties of heavy section Machinable Austempered Ductile Cast Iron (MADI). Mater Res Express 2019;6(6):066522.

[17] Lopes CL. Estudo da influência da microestrutura na cinética de austenitização na zona crítica e propriedades mecânicas de ferros nodulares austemperados duais tese. Universidade Federal de Santa Catarina; 2014.
[18] Guesser WL, Lopes CL, Bernardini PAN. Austempered ductile iron with dual microstructures: effect of initial microstructure on the austenitizing process. Int. J. Met. 2020;14(3):717–27.
[19] A. P. Druschitz, M. Ostrander, and R. Aristizabal, "The science of intercritically austempered ductile iron (IADI)," 71st world foundry congress, 19-21, [Bilbao Spain].
[20] Machado HD, Aristizabal-Sierra R, Garcia-Mateo C, Toda-Caraballo I. Effect of the starting microstructure in the formation of austenite at the intercritical range in ductile iron alloyed with nickel and copper. Int. J. Met. 2020;14(3):836–45.
[21] Abdollahi P, Amirsadeghi A, Kheirandish S, Mirdamadi S. Formation kinetics of austenite in pearlitic ductile iron. International Journal of Minerals, Metallurgy and Materials 2012;19(6):506–10.
[22] Vázquez-Gómez O, Barrera-Godínez JA, Vergara-Hernández HJ. Kinetic study of austenite formation during continuous heating of unalloyed ductile iron. International Journal of Minerals, Metallurgy, and Materials 2015;22(1):27–31.
[23] Batra U, Ray S, Prabhakar SR. Mathematical model for austenitization kinetics of ductile iron. J Mater Eng Perform 2005;14(October):574–81.
[24] ASTM A897/A897M – 16. Standard specification for austempered ductile iron castings. ASTM; 2016. p. 1–11.
[25] ASTM A247 - 16a. A247. Standard test method for evaluating the microstructure of graphite in iron castings, vol. 67; 2016. p. 1–13. Reapproved.
[26] ASTM E562. Standard test method for determining volume fraction by systematic manual point count. 2011. p. 1–7. Practice, no. C.
[27] Fisher GL. A method for obtaining quantitative dilatometric data from alloys undergoing a phase transformation. ldetallography 1970;3:229–33.
[28] Avrami M. Kinetics of phase change. II - transformation-time relations for random distribution of nuclei. J Chem Phys 1940;8(1940):212–24.
[29] Lis J, Lis a. Kinetics of the austenite formation during intercritical annealing. J. Achiev. Mater. 2008;26(2):195–8.
[30] Nelder JA, Mead R. A simplex method for function minimization. Comput J 1965;7:308–13.
[31] Suh DW. Dilatometric analysis of austenite formation during intercritical annealing. Met Mater Int 2008;14(3):275–82.
[32] Kop TA, Sietsma J, Van Der Zwaag S. Dilatometric analysis of phase transformations in hypo-eutectoid steels. J Mater Sci 2001;36(2):519–26.
[33] Martín DS, Caballero FG, Capdevila C, de Andrés CG. A model to estimate microstructural parameters from high resolution dilatometry data. International Conference on Advanced Steels (ICAS) 2010;1(October 2015).
[34] Caballero FG, Capdevila C, García de Andrés C. Modeling of the interlamellar spacing of isothermally formed pearlite in a eutectoid steel. Scripta Mater 2000;42(6):537–42.
[35] Lacaze J, Boudot A, Gerval V, Oquab D, Santos H. The role of manganese and copper in the eutectoid transformation of spheroidal graphite cast iron. Metall. Mater. Trans. A Phys. Metall. Mater. Sci. 1997;28(10):2015–25.
[36] Gerval V, Lacaze J. Critical temperature range in spheroidal graphite cast irons. ISIJ Int 2000;40(4):356–92.
[37] Gerval V, Siclari R, Lacaze J. Modelling continuous cooling transformation diagrams of spheroidal graphite cast irons. Int. J. Cast Met. Res. 1999;11(6):477–82.
[38] Caballero FG, Capdevila C, De Andrés CG. Mathematical modeling of iron and steel making processes. Modelling of kinetics of austenite formation in steels with different initial microstructures. ISIJ Int 2001;41(10):1093–102.
[39] De Andrés CG, Capdevila FGCC. Estudio dilatométrico de la descomposición anisotérmica de la perlita en un acero bajo en carbono (0,HC-0,50Mn). Rev. Metal. Madrid 1998;34(c):243–8.
[40] Erdogan M, Kilicli V, Demir B. Transformation characteristics of ductile iron austempered from intercritical austenitizing temperature ranges. J Mater Sci 2009;44(5):1394–403.
[41] Lacaze J, Sertucha J, Magnusson Åberg L. Microstructure of as-cast ferritic-pearlitic nodular cast irons. ISIJ Int 2016;56(9):1606–15.
[42] Gao M, Qu Y, Li G, You J, Li R. Cementites decomposition of a pearlitic ductile cast iron during graphitization annealing heat treatment. J Iron Steel Res Int 2017;24(8):838–43.